Progress In Electromagnetics Research B, Vol. 21, 129–150, 2010

SCATTERING OF MONOCHROMATIC ELECTROMAGNETIC WAVES ON 3D-DIELECTRIC BODIES OF ARBITRARY SHAPES

S. Kanaun

Mechanical Engineering Department, ITESM-CEM
Carretera Lago de Guadalupe 4 km
Atizapan, Edo de México 52926, México

Abstract—The work is devoted to the problem of scattering of monochromatic electromagnetic waves on heterogeneous dielectric inclusions of arbitrary shapes. For the numerical solution of the problem, the volume integral equation for the electric field in the region occupied by the inclusion is used. Discretization of this equation is carried out by Gaussian approximating functions. For such functions, the elements of the matrix of the discretized problem are calculated in explicit analytical forms. For a regular grid of approximating nodes, the matrix of the discretized problem proves to have the Toeplitz structure, and the matrix-vector product with such matrices can be carried out by the Fast Fourier Transform technique. The latter strongly accelerates the process of the iterative solution of the discretized problem. Electric fields inside a spherical inclusion and its differential cross-sections are calculated and compared with the exact (Mie) solution for various wave lengths of the incident field. Internal electric fields and the differential cross-sections of a cylindrical inclusion are calculated for the incident fields of various directions and wave lengths.

1. INTRODUCTION

The problem of scattering of electromagnetic waves on dielectric inclusions of arbitrary shapes has many important applications (see, e.g., [1]). That is why it has been in the focus of interest of many researches for several decades. Surveys of the numerical methods of the solution of this problem may be found in [2–4]. Some more recent

Corresponding author: S. Kanaun (kanaoun@itesm.mx).

methods are described in [5, 6]. Among these methods, the methods based on the volume integral equation of electromagnetics have a number of advantages. This equation reduces the scattering problem to the calculation of the electromagnetic field inside the inclusion only. The scattered field in the medium is expressed through the inside field with the help of a known integral operator. Existence and uniqueness of the solution of the volume integral equation of electromagnetics were proved in [4]. In [3, 4], a method of the numerical solution of this equation was also outlined. In this method, discretization of the volume integral equation is proposed to carry out by a set of identical approximating functions centered at the nodes of a regular grid. As a result, the matrix of the discretized problem obtains the Toeplitz properties, and the matrix-vector product with such a matrix may be carried out by the Fast Fourier Transform (FFT) technique. The latter accelerates essentially the process of iterative solution of the discretized problem.

In the present work, the discretization on the 3D-integral equation of the scattering problem is carried out by Gaussian approximating functions. The theory of approximation by the Gaussian and similar functions was developed in [7]. The main advantage of these functions is that the elements of the matrix of the discretized problem are calculated in explicit analytical forms, and numerical integration is not involved in the process of construction of this matrix. The Gaussian functions were used for the numerical analysis of static electric fields in a medium with a heterogeneous inclusion in [8].

The structure of the paper is as follows. In Section 2, the volume integral equation for the electric field inside a heterogeneous inclusion of arbitrary shape and the properties of the integral operator in this equation are discussed. In Section 3, discretization of this equation by Gaussian approximating functions is performed. Explicit equations for the elements of the matrix of the discretized problem and long-distance asymptotics of these equations are obtained in this section. In Section 4, the results of the numerical solution of the scattering problem for a spherical inclusion are compared with the exact (Mie) solution for various wave lengths of the incident field. The graphs of the electric fields inside the inclusion and the diffirential cross-sections of the latter are presented in this section. The scattering problem for a cylindrical inclusion arbitrary oriented with respect to the incident field is also considered in this section. Some features of the proposed method and the area of its application are discussed in the conclusion.

2. INTEGRAL EQUATION FOR ELECTROMAGNETIC WAVES IN A HOMOGENEOUS MEDIUM WITH AN ISOLATED INCLUSION

Consider an infinite homogeneous medium with dielectric properties described by a two-rank symmetric tensor C^0_{ij}. The medium contains an isolated inclusion that occupies a region V, and the dielectric properties inside V are defined by the tensor $C_{ij}(x)$, $x(x_1, x_2, x_3)$ is a point of the medium, and $\mathbf{x}$ is the vector of this point. The tensor of the dielectric properties of the medium with the inclusion is presented in the form

$$C_{ij}(x) = C^0_{ij} + C^1_{ij}(x)V(x),\ C^1_{ij}(x) = C_{ij}(x) - C^0_{ij}, \tag{1}$$

where $V(x)$ is the characteristic function of the region occupied by the inclusion:

$$V(x) = 1 \quad \text{if } x \in V, \quad V(x) = 0 \quad \text{if} \quad x \notin V. \tag{2}$$

Let an incident electric field $\mathbf{E}^0(x,t)$

$$\mathbf{E}^0(x,t) = \mathbf{U}^0(x)e^{i\omega t},\ \mathbf{U}^0(x) = \mathbf{A}^0 e^{-ik_0(\mathbf{n}^0\cdot\mathbf{x})} \tag{3}$$

propagate in the medium and be scattered on the inclusion V. Here ω is frequency, t is time, k_0 is the wave number of the incident field, $\mathbf{n}^0$ is its wave normal, and $\mathbf{n}^0\cdot\mathbf{x}$ is the scalar product of the vectors $\mathbf{n}^0$ and $\mathbf{x}$. $\mathbf{A}^0$ is the polarization vector of the incident field. In this case, the electric field $\mathbf{E}(x,t)$ in the medium with the inclusion has the form $\mathbf{E}(x,t) = \mathbf{U}(x)e^{i\omega t}$, and its amplitude $\mathbf{U}(x)$ satisfies the following integral equation (see e.g., [3, 4])

$$U_i(x) - \int G_{ij}(x-x')C^1_{jk}(x')U_k(x')V(x')dx' = U^0_i(x). \tag{4}$$

Here and farther, vectors and tensors are denoted by bold letters, for the components of vectors and tensors, the corresponding non-bold letters with low indices are used, summation with respect to repeating indices is implied.

Equation (4) serves for a set of inclusions as well as for an isolated inclusion in an infinite homogeneous medium. For an isotropic medium, $C^0_{ij} = c_0\delta_{ij}$ (c_0 is a scalar, δ_{ij} is the Kronecker symbol) and the kernel $G_{ij}(x)$ of the integral operator in this equation takes the form

$$G_{ij}(x) = k_0^2 g(x)\delta_{ij} + \partial_i\partial_j g(x), \quad \partial_i = \frac{\partial}{\partial x_i}, \tag{5}$$

$$g(x) = \frac{e^{-ik_0|x|}}{4\pi c_0|x|}, \qquad k_0^2 = \omega^2 c_0. \tag{6}$$

Thus, the kernel $\mathbf{G}(x)$ is the second derivative of the function $g(x)$ that has a weak singularity.

Equation (4) was considered by many authors and is in essence the equation for the field $\mathbf{U}(x)$ inside the inclusion (in the region V). The field outside V may be reconstructed from the same Eq. (4) if $\mathbf{U}(x)$ inside V is known. Note that integration in Eq. (4) may be formally spread over any region W that includes V. For instance in Section 3, the numerical solution of this equation is constructed in a minimal cuboid W that includes V.

Note that Eq. (4) may be rewritten in the form

$$\mathbf{U}(x) = \mathbf{U}^0(x) + \mathbf{U}^s(x), \quad \mathbf{U}^s(x) = \int\limits_V \mathbf{G}(x-x') \cdot \mathbf{C}^1(x') \cdot \mathbf{U}(x') dx', \quad (7)$$

where $\mathbf{U}^s(x)$ is the electric field scattered on the inclusion. In the far zone ($|\mathbf{x}| \gg L$, L is a characteristic size of the inclusion) the following asymptotic representations hold:

$$|x - x'| \approx |\mathbf{x}| - \mathbf{n} \cdot \mathbf{x}', \quad \mathbf{n} = \frac{\mathbf{x}}{|\mathbf{x}|}, \quad (8)$$

$$g(x - x') \approx \frac{e^{-ik_0|x|}}{4\pi c_0 |x|} e^{ik_0(\mathbf{n}\cdot\mathbf{x}')}, \quad (9)$$

$$\partial_i \partial_j g(x - x') \approx -k_0^2 n_i n_j \frac{e^{-ik_0|x|}}{4\pi c_0 |x|} e^{ik_0(\mathbf{n}\cdot\mathbf{x}')}, \quad (10)$$

and the field $\mathbf{U}^s(x)$ takes the form

$$U_i^s(x) \approx \frac{e^{-ik_0|x|}}{4\pi c_0 |x|} F_i(\mathbf{n}), \quad (11)$$

$$F_i(\mathbf{n}) = k_0^2 (\delta_{ij} - n_i n_j) \int\limits_V C_{jk}^1(x') U_k(x') e^{ik_0(\mathbf{n}\cdot\mathbf{x}')} dx'. \quad (12)$$

Here $\mathbf{F}(\mathbf{n})$ is called the amplitude of the scattered field. If the direction $\mathbf{n}$ coincides with $\mathbf{n}^0$ (the direction of the incident field propagation), $\mathbf{F}(\mathbf{n}^0)$ is the forward scattered amplitude. The square of the module $|\mathbf{F}(\mathbf{n})|^2$ of the complex vector $\mathbf{F}(\mathbf{n})$ in Eq. (12) is proportional to the so-called differential scattering cross-section of the inclusion [1], and according to (12) $|\mathbf{F}(\mathbf{n})|^2$ takes the form

$$|\mathbf{F}(\mathbf{n})|^2 = k_0^4 \left[\left| \widehat{\mathbf{U}} \right|^2 - \left| \mathbf{n} \cdot \widehat{\mathbf{U}} \right|^2 \right], \quad (13)$$

$$\widehat{\mathbf{U}} = \int\limits_V \mathbf{C}^1(x') \cdot \mathbf{U}(x') e^{ik_0(\mathbf{n}\cdot\mathbf{x}')} dx'. \quad (14)$$

Farther, we define the normalized differential scattering cross-section $q(\mathbf{n})$ of an inclusion by the following equation

$$q(\mathbf{n}) = \frac{|\mathbf{F}(\mathbf{n})|^2}{|\mathbf{F}(\mathbf{n}^0)|^2}. \tag{15}$$

3. NUMERICAL SOLUTION OF THE INTEGRAL EQUATIONS (4)

3.1. Gaussian Approximating Functions

For the numerical solution of Eq. (4), this integral equation should be firstly discretized using an appropriate class of approximating functions (see, e.g., [9]). In this work, the Gaussian approximation functions are used for this purpose. According to [7], a bounded smooth function $u(x)$ defined on 3D-space can be presented in the form of the following series:

$$u(x) \approx u_h(x) = \sum_r u^{(r)} \varphi\left(x - x^{(r)}\right), \quad \varphi(x) = \frac{1}{(\pi H)^{3/2}} \exp\left(-\frac{|x|^2}{Hh^2}\right). \tag{16}$$

Here $x^{(r)}$ $(r = 1, 2, \ldots)$ are the nodes of a regular node grid. The vector $\mathbf{x}^{(r)}$ of the node $x^{(r)}$ has the components $(hm,\ hn,\ hp)$, where m, n, p are integers (connection between the indices r and $m,\ n,\ p$ is indicated below), h is the step of the node grid, $u^{(r)} = u(x^{(r)})$ is the value of function $u(x)$ in the node $x^{(r)}$, and H is a non-dimensional parameter of the order 1. In [7], Eq. (16) is called the "approximate approximation" because its error does not vanish when $h \to 0$. But the non-reducing part of the error has the order of $\exp(-\pi^2 H)$ and may be neglected in practical calculations.

3.2. Discretization of the Integral Equation (4)

Let us take a cuboid W that contains the region V occupied by the inclusion and cover W by a regular grid of approximating nodes at points $x^{(r)}$ $(r = 1, 2, \ldots, N)$ (see Fig. 1). The solution of Eq. (4) in W is approximated by the series (16), where the Gaussian functions φ are centered at the node points $x^{(r)}$

$$U_i(x) \approx \sum_{r=1}^{N} U_i^{(r)} \varphi\left(x - x^{(r)}\right). \tag{17}$$

Here N is the total number of the nodes in W, $U_i^{(r)}$ are unknown coefficients of the approximation. Upon substitution of (17) into

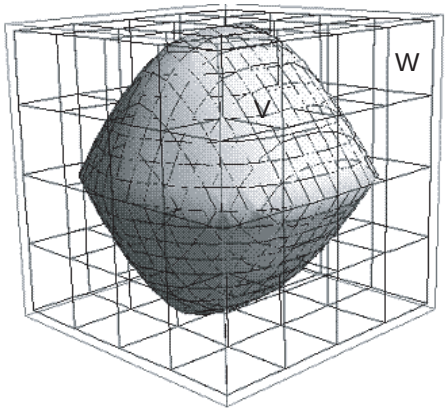

Figure 1. An inclusion V inside a cuboid W covered with a regular grid of approximating nodes.

Eq. (4) we obtain:

$$U_i(x) - \sum_{s=1}^{N} \Gamma_{ij}\left(x - x^{(r)}\right) C_{jk}^{1(r)} U_k^{(r)} = U_i^0(x), \tag{18}$$

where

$$\Gamma_{ij}(x) = \int G_{ij}(x - x')\varphi(x')dx', \quad C_{ij}^{1(r)} = C_{ij}^{1}\left(x^{(r)}\right). \tag{19}$$

It follows from Eq. (5) for $\mathbf{G}(x)$ that the tensor $\mathbf{\Gamma}(x)$ is presented in the form

$$\Gamma_{ij}(x) = k_0^2 \gamma_0(x)\delta_{ij} + \partial_i \partial_j \gamma_0(x), \tag{20}$$

$$\gamma_0(x) = \int g(x - x')\varphi(x')dx', \tag{21}$$

where the function $g(x)$ has form (6). The integral $\gamma_0(x)$ has a weak (integrable) singularity, and its direct calculation leads to the following equation ($\varsigma = |x|/h,\ \kappa_0 = k_0 h$)

$$\gamma_0(x) = \frac{h^2}{8\pi c_{0\varsigma}} \exp\left[-\frac{H\kappa_0^2 + 4i\varsigma\kappa_0}{4}\right] \left[\mathrm{Erfc}\left(\frac{iH\kappa_0 - 2\varsigma}{2\sqrt{H}}\right) - e^{2i\kappa_0\varsigma}\mathrm{Erfc}\left(\frac{iH\kappa_0 + 2\varsigma}{2\sqrt{H}}\right)\right]. \tag{22}$$

Here $\mathrm{Erfc}\,(z)$ is the complimentary error function of a complex argument

$$\mathrm{Erfc}\,(z) = 1 - \mathrm{Erf}(z), \quad \mathrm{Erf}(z) = \frac{2}{\sqrt{\pi}} \int\limits_0^z e^{-t^2} dt. \tag{23}$$

After calculating two derivatives of the integral $\gamma_0(x)$ and substituting the result into Eq. (20) the integral $\Gamma_{ij}(x)$ takes the form

$$\Gamma_{ij}(x) = \frac{1}{c_0} \left(\gamma_1(\varsigma)\delta_{ij} + \gamma_2(\varsigma) n_i n_j\right), \quad n_i = \frac{x_i}{|\mathbf{x}|}. \tag{24}$$

Here two scalar functions γ_1, γ_2 are as follows

$$\begin{aligned}\gamma_1(\varsigma) = \frac{1}{8\,(\pi H)^{3/2}\,\varsigma^3} \Bigg\{ & 4\varsigma \exp\left(-\frac{\varsigma^2}{H}\right) - \sqrt{\pi H} \exp\left(-\frac{H\kappa_0^2}{4}\right) \\ & \Bigg[\exp\left(-i\kappa_0\varsigma\right)\left(1 + \kappa_0\varsigma(i - \kappa_0\varsigma)\right)\mathrm{Erfc}\left(\frac{iH\kappa_0 - 2\varsigma}{2\sqrt{H}}\right) \\ & + \exp(i\kappa_0\varsigma)(1 - \kappa_0\varsigma(i + \kappa_0\varsigma))\mathrm{Erfc}\left(\frac{iH\kappa_0 + 2\varsigma}{2\sqrt{H}}\right)\Bigg]\Bigg\}, \end{aligned} \tag{25}$$

$$\begin{aligned}\gamma_2(\varsigma) = \frac{1}{8\,(\pi H)^{3/2}\,\varsigma^3} \Bigg\{ & -4\varsigma \exp\left(-\frac{\varsigma^2}{H}\right)(3H + 2\varsigma^2) + H\sqrt{\pi H} \exp\left(-\frac{H\kappa_0^2}{4}\right) \\ & \Bigg[\exp(-i\kappa_0\varsigma)\left(3 + \kappa_0\varsigma(3i - \kappa_0\varsigma)\right)\mathrm{Erfc}\left(\frac{iH\kappa_0 - 2\varsigma}{2\sqrt{H}}\right) \\ & - \exp(i\kappa_0\varsigma)(3 - \kappa_0\varsigma(3i + \kappa_0\varsigma))\mathrm{Erfc}\left(\frac{iH\kappa_0 + 2\varsigma}{2\sqrt{H}}\right)\Bigg]\Bigg\}. \end{aligned} \tag{26}$$

Asymptotics $\overline{\gamma}_1(\varsigma)$, $\overline{\gamma}_2(\varsigma)$ of these functions for large values of the argument ς have the forms

$$\overline{\gamma}_1(\varsigma) = \frac{1}{4\pi\varsigma^3} \exp\left[-\frac{1}{4}\left(H\kappa_0^2 + 4i\varsigma\kappa_0\right)\right]\left[(\kappa_0\varsigma)^2 - 1 - i\kappa_0\varsigma\right], \tag{27}$$

$$\overline{\gamma}_2(\varsigma) = -\frac{1}{4\pi\varsigma^3} \exp\left[-\frac{1}{4}\left(H\kappa_0^2 + 4i\varsigma\kappa_0\right)\right]\left[(\kappa_0\varsigma)^2 - 3 - 3i\kappa_0\varsigma\right]. \tag{28}$$

The graphs of the real and imaginary parts of the functions $\gamma_1(\varsigma)$ and $\gamma_2(\varsigma)$ (solid lines) and their asymptotic expressions $\overline{\gamma}_1(\varsigma)$ and $\overline{\gamma}_2(\varsigma)$ (dashed lines) are presented in Figs. 2 and 3 for $\kappa_0 = 0.5, 1, 2$. It is seen that the real parts of these functions and their asymptotics coincide when $\varsigma > 4$. Meanwhile, their imaginary parts practically coincide for all values of ς. Thus, for large values of ς, the asymptotic Equations (27), (28) for the functions γ_1, γ_2 can be used instead of the complete Equations (25), (26).

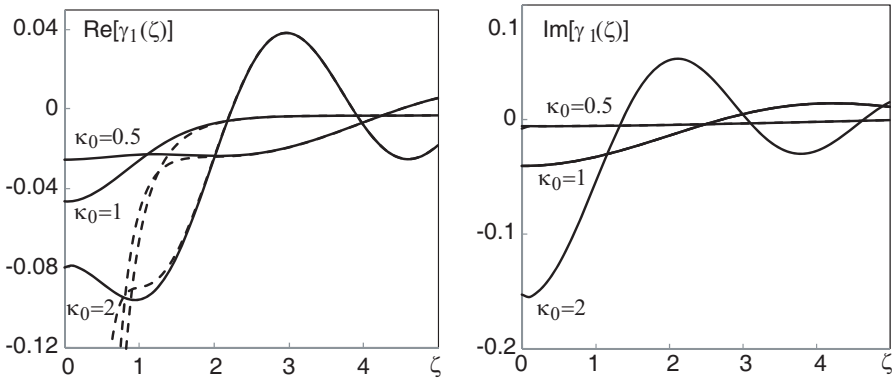

Figure 2. Real and imaginary parts of the function $\gamma_1(\varsigma)$ in Eq. (25) for various values of the parameter $\kappa_0 = k_0 h$ (solid lines), and the long-distance asymptotic $\overline{\gamma}_1(\varsigma)$ of this function in Eq. (27) (dashed lines).

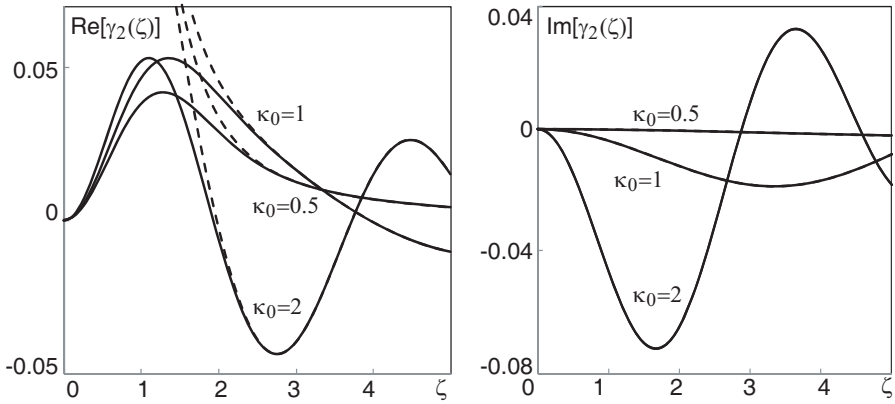

Figure 3. Real and imaginary parts of the function $\gamma_2(\varsigma)$ in Eq. (26) for various values of the parameter $\kappa_0 = k_0 h$ (solid lines), and the long-distance asymptotic $\overline{\gamma}_2(\varsigma)$ of this function in Eq. (28) (dashed lines).

The system of linear algebraic equations for the unknowns $U_i^{(r)}$ in Eq. (17) follows from Eq. (18) if the latter is satisfied at all the nodes $x^{(r)}$ (the Collocation Method [9]). Note that if the nodes of the approximation (17) constitute a cubic grid, the coefficients of the approximation $U_i^{(r)}$ coincide with the values of $U_i(x)$ at the

corresponding nodes ($U_i^{(r)} = U_i(x^{(r)})$, $r = 1, 2, \ldots, N$) (see [7]). As a result, we obtain the following system of linear algebraic equations for the coefficients $U_i^{(r)}$

$$U_i^{(r)} - \sum_{s=1}^{N} \Gamma_{ij}^{(r,s)} C_{jk}^{1(s)} U_k^{(s)} = U_i^{0(r)}, \ r = 1, 2, \ldots, N; \tag{29}$$

$$\Gamma_{ij}^{(r,s)} = \Gamma_{ij}\left(x^{(r)} - x^{(s)}\right), \ U_i^{0(r)} = U_i^0\left(x^{(r)}\right), \tag{30}$$

where $\Gamma_{ij}(x)$ is defined in Eq. (24). The matrix form of these equations is

$$(\mathbf{I} - \mathbf{B})\mathbf{X} = \mathbf{F}, \tag{31}$$

where $\mathbf{I}$ is the unit matrix of the dimensions $3N \times 3N$, the vector of unknowns $\mathbf{X}$ and of the right hand side $\mathbf{F}$ have the dimensions $3N$

$$\mathbf{X} = \left|X^1, X^2, \ldots, X^{3N}\right|^T, \ \mathbf{F} = \left|F^1, F^2, \ldots, F^{3N}\right|^T, \tag{32}$$

$$\begin{aligned} X^r &= \begin{cases} U_1^{(r)}, & r \le N \\ U_2^{(r-N)}, & N < r \le 2N \\ U_3^{(r-2N)}, & 2N < r \le 3N \end{cases}, \\ F^r &= \begin{cases} U_1^{0(r)}, & r \le N \\ U_2^{0(r-N)}, & N < r \le 2N \\ U_3^{0(r-2N)}, & 2N < r \le 3N \end{cases}, \end{aligned} \tag{33}$$

$|\ldots|^T$ is the transposition operation. The matrix $\mathbf{B}$ in Eq. (31) has the dimensions $3N \times 3N$ and consists of 9 sub-matrices $\mathbf{b}_{ij}$ of the dimensions $N \times N$,

$$\mathbf{B} = \left| \begin{array}{ccc} \mathbf{b}_{11}, & \mathbf{b}_{12}, & \mathbf{b}_{13} \\ \mathbf{b}_{21}, & \mathbf{b}_{22}, & \mathbf{b}_{23} \\ \mathbf{b}_{31}, & \mathbf{b}_{32}, & \mathbf{b}_{33} \end{array} \right| \tag{34}$$

with elements b_{ij}^{rs} given by

$$b_{ij}^{rs} = \Gamma_{ik}^{(rs)} C_{kj}^{1(s)}, \quad i, j = 1, 2, 3; \ r, s = 1, 2, \ldots, N. \tag{35}$$

3.3. Iterative Solution of the System (31)

It follows from (29)–(35) and (24)–(28) that $\mathbf{B}$ in Eq. (31) is a non-sparse matrix which dimensions may be very large if high accuracy is required. For such linear algebraic systems, only iterative methods are efficient. For instance, if the minimal residual method (see, e.g., [4, 9])

is used, the n-th iteration $\mathbf{X}^{(n)}$ of the solution of Eq. (31) is calculated as follows:

$$\mathbf{X}^{(n)}=\mathbf{X}^{(n-1)}-\alpha\mathbf{Y}^{(n-1)},\ \ \alpha=\frac{\mathbf{Y}^{(n-1)}\cdot\left[(\mathbf{I}-\mathbf{B})\mathbf{Y}^{(n-1)}\right]}{\left[(\mathbf{I}-\mathbf{B})\mathbf{Y}^{(n-1)}\right]\cdot\left[(\mathbf{I}-\mathbf{B})\mathbf{Y}^{(n-1)}\right]}, \quad (36)$$

$$\mathbf{Y}^{(n)}=\mathbf{Y}^{(n-1)}-\alpha(\mathbf{I}-\mathbf{B})\mathbf{Y}^{(n-1)}, \quad (37)$$

with the initial values $\mathbf{X}^{(0)}, \mathbf{Y}^{(0)}$ of the vectors $\mathbf{X}$ and $\mathbf{Y}$

$$\mathbf{X}^{(0)}=\mathbf{F},\ \ \mathbf{Y}^{(0)}=-\mathbf{BF}. \quad (38)$$

In these equations

$$\mathbf{Y}\cdot\mathbf{Z}=\sum_{r=1}^{N}Y^r\widetilde{Z}^r,$$

where $\mathbf{Y}$ and $\mathbf{Z}$ are N-dimensional vectors with the complex components $Y^r$and Z^r, and $\widetilde{Z}^r$ is the complex conjugate number with respect to Z^r. Convergence of this method in the case of electromagnetic wave scattering problem is proved in [4].

It is seen from Eqs. (36), (37) that the vector $\mathbf{Y}^{(n-1)}$ is multiplied by the matrix $\mathbf{I}-\mathbf{B}$ at every step of the iteration process. For non-sparse matrices of large dimensions, calculation of such a product is an expensive computational operation. If, however, a regular grid of approximating nodes is used, the volume of the calculations is reduced substantially. Let us consider the product $\mathbf{BY}$ in the case of an isotropic inclusion. This product is a combination of the following sums

$$P_{ij}^{(r)}=\sum_{s=1}^{N}\Gamma_{ij}(x^{(r)}-x^{(s)})Z^s,\ \ Z^s=c_1^{(s)}Y^{(s+(j-1)N)}, \quad (39)$$

$$c_1^{(s)}=c(x^{(s)})-c_0;\ r,s=1,2,\ldots,N;\ \ i,j=1,2,3,$$

where the tensor $\Gamma_{ij}(x)$ is defined in Eq. (24), and $c(x)$ is the dielectric permittivity of the medium with the inclusion. For a regular node grid with a step h, the coordinates of every node $x^{(r)}$ can be presented in the form

$$x^{(r)}=\left(x_1^{(m)},x_2^{(n)},x_3^{(p)}\right), \quad (40)$$

$$x_1^{(m)}=L_1+hm,\ x_2^{(n)}=L_2+hn,\ x_3^{(p)}=L_3+hp. \quad (41)$$

Here $m,\ n,\ p=0,1,2,\ldots$ are integers, $L_1,\ L_2,\ L_3$ are minimal values of the node coordinates in the cuboid W which sides are parallel to

the axes $x_1,\ x_2,\ x_3$. Thus, the position of every node may be defined by 3 indices (m, n, p). Connection between the one and three-index numerations of the nodes may be introduced by the equation

$$r(m,n,p) = m + N_1(n-1) + N_1N_2(p-1), \tag{42}$$
$$1 \le m \le N_1,\ 1 \le n \le N_2,\ 1 \le p \le N_3.$$

Here $N_1,\ N_2,\ N_3$ are the number of the nodes along the corresponding sides of W. In the three-index numeration, the sum (39) is presented in the form

$$P_{ij}^{r(m,n,p)} = \sum_{l=1}^{N_1}\sum_{q=1}^{N_2}\sum_{t=1}^{N_3}\Gamma_{ij}\left(x_1^{(m)}-x_1^{(l)}, x_2^{(n)}-x_2^{(q)}, x_3^{(p)}-x_3^{(t)}\right)\overline{Z}^{(l,q,t)},$$
$$\overline{Z}^{(l,q,t)} = Z^{r(l,q,t)}, \tag{43}$$

where

$$\Gamma_{ij}\left(x_1^{(m)} - x_1^{(l)}, x_2^{(n)} - x_2^{(q)}, x_3^{(p)} - x_3^{(t)}\right)$$
$$= \Gamma_{ij}(h(m-l), h(n-q), h(p-t)). \tag{44}$$

It is seen from the last equation that the object $\Gamma_{ij}(x_1^{(m)} - x_1^{(p)}, x_2^{(n)} - x_2^{(q)}, x_3^{(p)} - x_3^{(t)})$ has the Toeplitz structure: it depends on the differences of the indices: $m - p$, $n - q$, and $p - t$. As a result, the Fourier transform technique can be used for the calculation of the triple sums in Eq. (43) and therefore, for the matrix-vector products. Application of the FFT algorithms for calculation of these sums essentially accelerates the iterative process (36)–(38). In addition, one has to keep in the computer memory not all the matrices $\Gamma_{ij}^{(r,s)}$ of the dimensions $(N_1N_2N_3) \times (N_1N_2N_3)$ but only one column and one row of these matrices: the objects that have the dimensions $(2N_1 \times 2N_2 \times 2N_3)$ and are calculated once for all the iteration process. The details of the FFT algorithm for the calculation of the matrix-vector products are described in [10, 11].

4. NUMERICAL RESULTS

Let us start with a spherical inclusion of the radius a and consider the electric field inside it in the Cartesian coordinate system with the origin in the center of the inclusion and the axes x_1 and x_3 directed along the polarization vector $\mathbf{U}^0$ and the wave normal $\mathbf{n}^0$ of the incident field (Fig. 4). The medium and the inclusion are isotropic with the dielectric permittivities c_0 and c, correspondingly. In the calculations, we take $c/c_0 = 2$. In the non-dimensional variables $\varsigma_i = x_i/a$ $(i = 1, 2, 3)$,

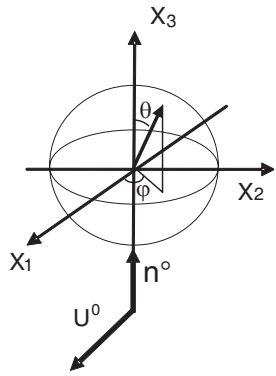

Figure 4. A spherical inclusion and the directions of the wave normal $\mathbf{n}^0$ and the polarization vector $\mathbf{U}^0$ of the incident field.

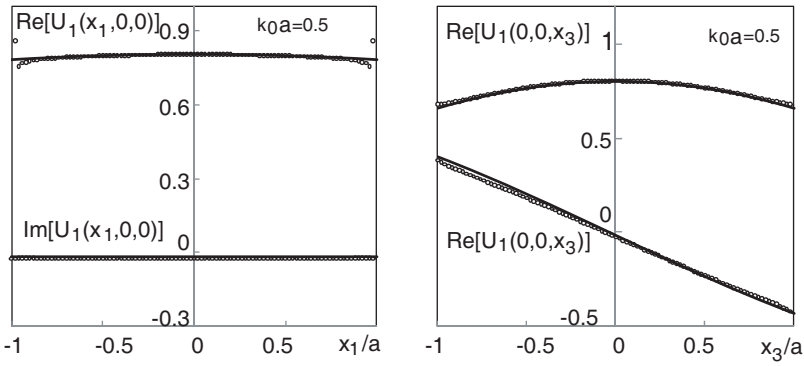

Figure 5. Real and imaginary parts of the component U_1 of the electric field inside a spherical inclusion of the radius a for the wave number of the incident field $k_0 a = 0.5$ ($c/c_0 = 2$); the function $U_1(x_1, 0, 0)$ is in the left figure, the function $U_1(0, 0, x_3)$ is in the right figure. Solid lines correspond to the exact (Mie) solutions, lines with white dots are numerical solutions for a cubic node grid with the step $h = 0.02$.

the radius of the inclusion becomes equal to 1, and the integral Eq. (4) keeps its form if the wave number k_0 is replaced by the non-dimensional wave number $k_0 a$. The distribution of the real ($\mathrm{Re}U_1$) and imaginary ($\mathrm{Im}U_1$) parts of the component $U_1(\varsigma_1, \varsigma_2, \varsigma_3)$ of the vector $\mathbf{U}$ along the ς_1 and ς_3-axes are presented in Figs. 5, 7, 9 and 11 for the non-dimensional wave number of the incident field $k_0 a = 0.5, 1, 2, 5$. In this figure, solid lines correspond to the exact (Mie) solution (see, e.g., [1]),

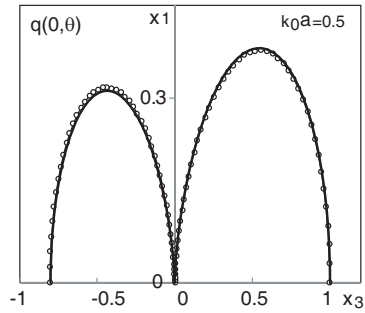

Figure 6. The diagram of the normalized differential cross-section $q(\phi, \theta)$ of a spherical inclusion of the radius a for the wave number of the incident field $k_0 a = 0.5$. Solid line corresponds to the exact diagram (Mie's solution), line with white dots is the numerical solution for a cubic node grid with the step $h = 0.02$.

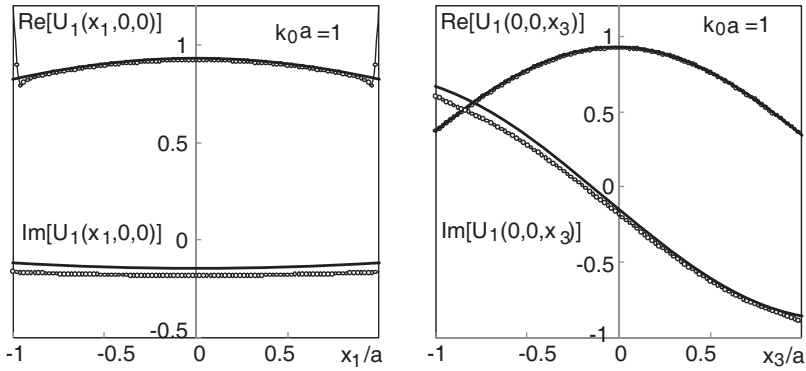

Figure 7. The same as in Fig. 5 for $k_0 a = 1$.

and lines with white dots to the numerical solution described in the previous section for the grid step $h = 0.02$ (the total number of the nodes $N = 1030301$). For the mentioned values of $k_0 a$, the graphs of the normalized differential cross-section $q(\phi, \theta)$ defined in Eq. (15) are in Figs. 6, 8, 10, and 12. (Here ϕ and θ are the angels of the spherical coordinate system with the polar axis x_3 (Fig. 4). These angles define the direction of the vector $\mathbf{n}$ in Eq. (15) for $q(\mathbf{n})$.) Because of the symmetry of the problem, the normalized differential cross-section q does not depend on the angle φ, and the diagrams in Figs. 6, 8, 10, 12 are parametrically defined by the equations: $x_1 = q(0, \theta) \sin(\theta)$, $x_3 = q(0, \theta) \cos(\theta)$.

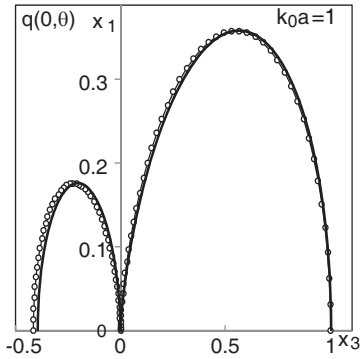

Figure 8. The same as in Fig. 6 for $k_0a = 1$.

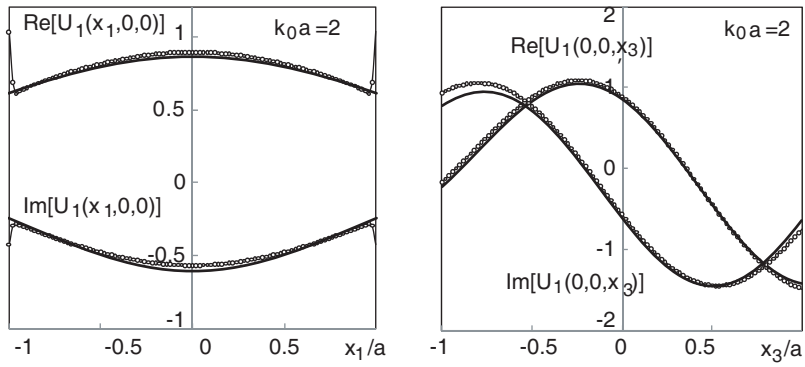

Figure 9. The same as in Fig. 5 for $k_0a = 2$.

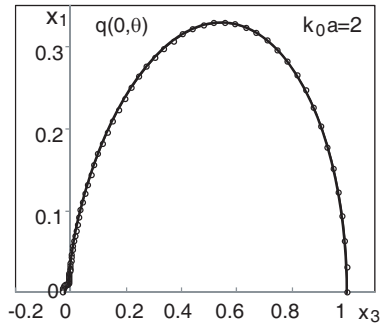

Figure 10. The same as in Fig. 6 for $k_0a = 2$.

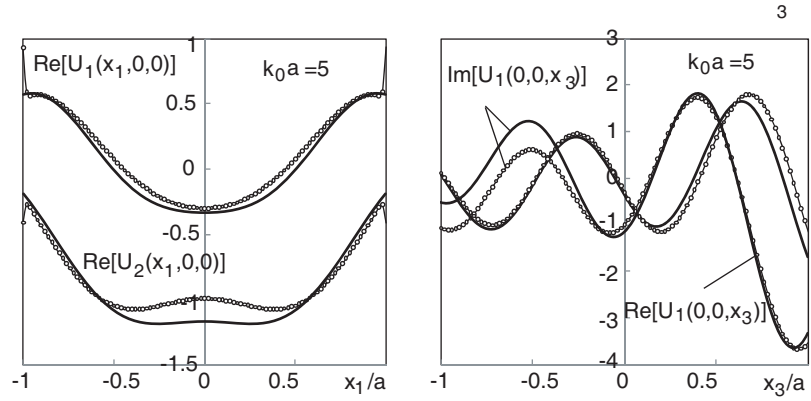

Figure 11. The same as in Fig. 5 for $k_0a = 5$.

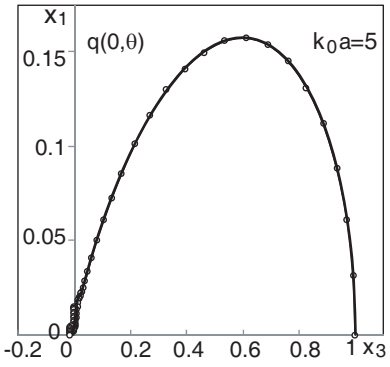

Figure 12. The same as in Fig. 6 for $k_0a = 5$.

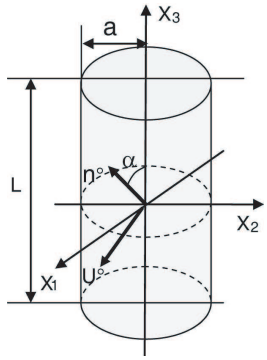

Figure 13. A cylindrical inclusion and the directions of the wave normal $\mathbf{n}^0$ and the polarization vector $\mathbf{U}^0$ of the incident field.

The integral relative error Δ of the numerical solution may be introduced by the following equation

$$\Delta = \left(\int\limits_V |\mathbf{E}^e(x)|\, dx \right)^{-1} \int\limits_V \left| \mathbf{E}^h(x) - \mathbf{E}^e(x) \right| dx. \tag{45}$$

Here $\mathbf{E}^h(x)$ is the numerical solution that corresponds to the step h of the node grid, $\mathbf{E}^e(x)$ is the exact solution. The function $\Delta(h)$ monotonically decreases if h decreases. For k_0a of the order 1, Δ changes from the value about 0.1 for $h = 0.1$ till $\Delta \approx 0.03$ for $h = 0.02$.

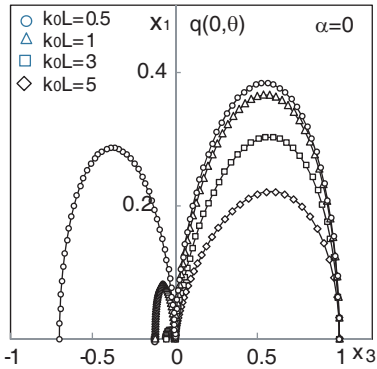

Figure 14. The diagram of the normalized differential cross-section $q(\phi, \theta)$ of a cylindrical inclusion of the length L and radius a ($L/a = 2$, $c/c_0 = 2$) for various wave numbers of the incident field $k_0 L = 0.5, 1, 3, 5$. The direction of the wave normal $\mathbf{n}^0$ coincides with the cylinder axis x_3 ($\alpha = 0$)

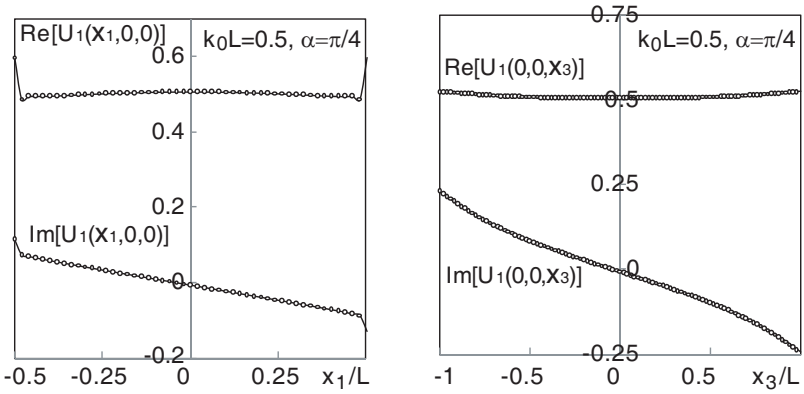

Figure 15. Real and imaginary parts of the component U_1 of the electric field inside a cylindrical inclusion of the length L and radius a ($L/a = 2$) for the wave number of the incident field $k_0 L = 0.5$ ($c/c_0 = 2$) and the angle between the wave normal n^0 and the cylinder axis $\alpha = \pi/4$; the function $U_1(x_1, 0, 0)$ is in the left figure, the function $U_1(0, 0, x_3)$ is in the right figure. Lines with white dots correspond to the numerical solution for a cubic node grid with the step $h = 0.02$.

For larger values of the wave numbers $k_0 a$ as well as for higher contrasts in the properties of the medium and the inclusion, Δ becomes larger, but it is always decreases together with h. The local error is maximal near the boundary of the body as it is seen in Figs. 5, 7, 9 and 11.

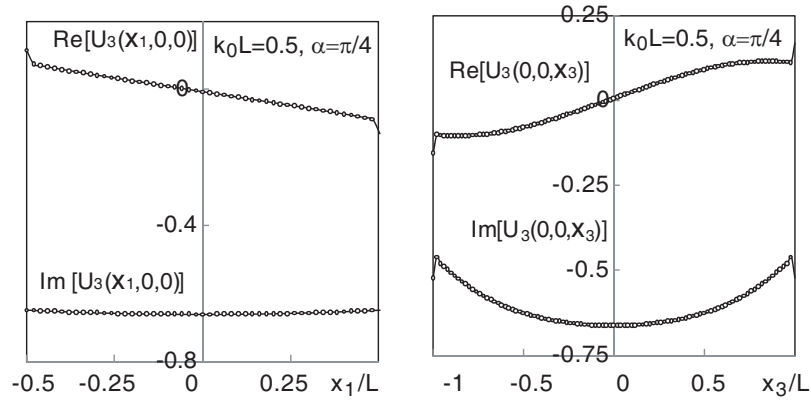

Figure 16. Real and imaginary parts of the component U_3 of the electric field inside a cylindrical inclusion of the length L and radius a ($L/a = 2$) for the wave number of the incident field $k_0L = 1$ ($c/c_0 = 2$) and the angle between its wave normal $\mathbf{n}^0$ and the cylinder axis $\alpha = \pi/4$; the function $U_3(x_1, 0, 0)$ is in the left figure, the function $U_3(0, 0, x_3)$ is in the right figure. Lines with white dots correspond to the numerical solution for a cubic node grid with the step $h = 0.02$.

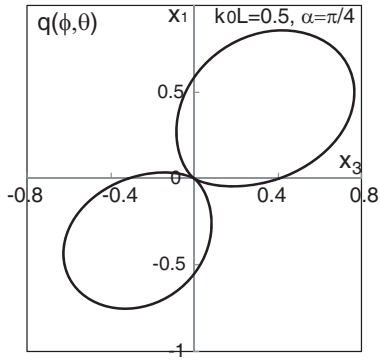

Figure 17. The diagram of the normalized differential cross-section $q(\phi, \theta)$ of a cylindrical inclusion of the length L and radius a ($L/a = 2$) for the wave number of the incident field $k_0L = 0.5$ and the angle of its wave normal $\mathbf{n}^0$ with the cylinder axis $\alpha = \pi/4$.

For $h > 0.01$, the numerical solution is not sensitive to the value of the parameter H in the approximation (16) if H is in the region $1 < H < 3$. Note that the parameter H should satisfy the condition $\exp(-\pi^2 H) < h$ (see [7]).

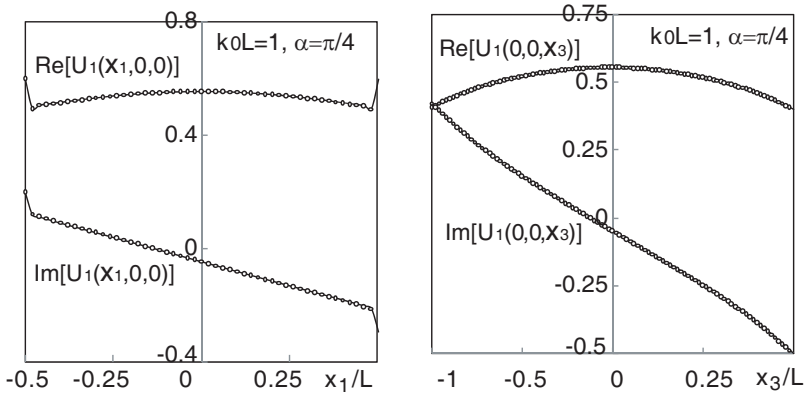

Figure 18. The same as in Fig. 15 for $k_0L = 1$.

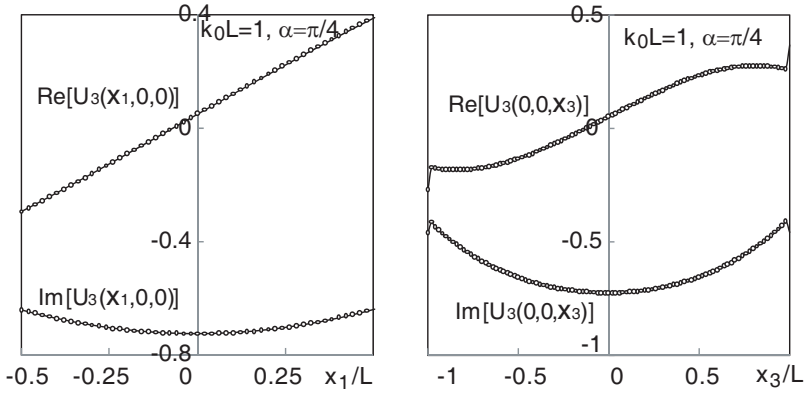

Figure 19. The same as in Fig. 16 for $k_0L = 1$.

The convergence of the proposed numerical methods depends on the contrast in the properties of the inclusion and the medium as well as on the value of the wave number of the incident field. For $|c/c_0| < 3$ and $k_0a < 3$, the tolerance $\varepsilon = 0.001$ ($\varepsilon = |\mathbf{X}^{(n)} - \mathbf{X}^{(n-1)}|/|\mathbf{X}^{(n)}|$) is achieved in 5 iterations. But the number of iterations may increase till several hundreds for large property contrasts or/and very short waves.

Let a monochromatic incident field be scattered on a dielectric cylindrical inclusion which length L is twice of its radius a. The dielectric permittivities of the medium and the cylinder are c_0 and c, and $c/c_0 = 2$. The angle between the wave normal $\mathbf{n}^0$ of the incident field and the axis x_3 of the cylinder is α (Fig. 13). Thus, the incident

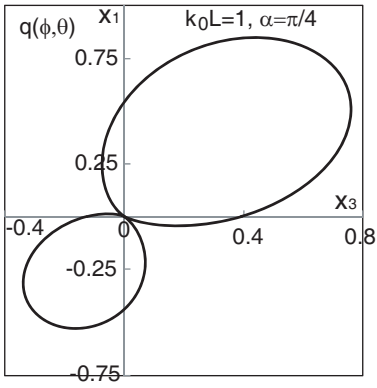

Figure 20. The same as in Fig. 17 for $k_0L = 1$.

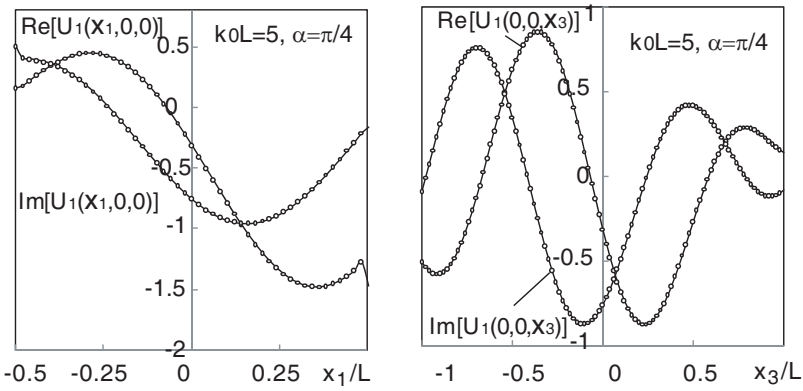

Figure 21. The same as in Fig. 15 for $k_0L = 5$.

field $\mathbf{U}^0(x_1, x_2, x_3)$ is defined by the equation

$$\mathbf{U}^0(x_1, x_2, x_3) = \left(\cos(\alpha)\,\mathbf{e}^1 - \sin(\alpha)\mathbf{e}^3\right) \exp[-ik_0\,(\sin(\alpha)x_1 + \cos(\alpha)x_3)]\,. \tag{46}$$

Here $\mathbf{e}^1$ and $\mathbf{e}^3$ are unit vectors of the axes x_1 and x_3. If $\alpha = 0$, the normalized differential cross-section $q(\phi, \theta)$ of the inclusion does not depend on the angle ϕ. The parametric graphs of the function $q(0, \theta)$ for various values of the non-dimensional wave number k_0L of the incident field are presented in Fig. 14.

The numerical results for the angle $\alpha = \pi/4$ are in Figs. 15–23 for the wave numbers of the incident field $k_0L = 0.5, 1, 5$. The graphs of the real and imaginary parts of the components U_1 and U_3 of the electric field inside the inclusion are in Figs. 15, 18 and 21 (U_1) and 16, 19 and

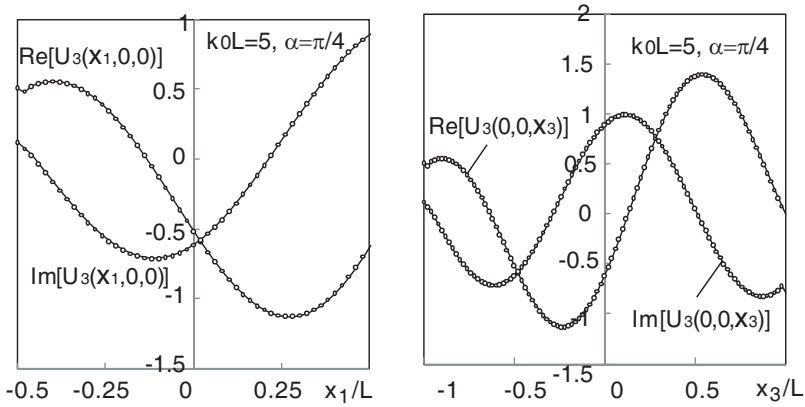

Figure 22. The same as in Fig. 16 for $k_0 L = 5$.

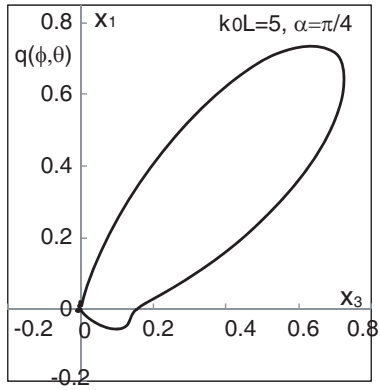

Figure 23. The same as in Fig. 17 for $k_0 L = 5$.

22 (U_3). The diagrams of the corresponding differential cross-sections are in Figs. 17, 20 and 23. For $x_1 > 0$, these graphs are parametrically defined by the equations: $x_1 = q(0,\theta)\sin(\theta)$, $x_3 = q(0,\theta)\cos(\theta)$, and for $x_1 < 0$, by the equations: $x_1 = -q(\pi,\theta)\sin(\theta)$, $x_3 = q(\pi,\theta)\cos(\theta)$.

5. CONCLUSION

The method proposed in this work is an efficient tool for the numerical solution of the electromagnetic wave scattering problems. It allows calculating electric fields inside heterogeneous inclusions of arbitrary shapes in a wide region of the wave lengths of the incident field and dielectric properties of the medium and the inclusion.

The method can be applied to the numerical solution of other problems of mathematical physics that can be reduced to volume integral equations (elastic wave diffraction problems, diffusion in the medium with inclusions, static fields in a homogeneous medium with inclusions, etc.). For discretization of the corresponding integral equations, the Gaussian approximating functions may be used. The advantage of these functions is that the elements of the matrix of the discretized problems are calculated in explicit analytical forms. For some problems of mathematical physics, these elements may not be calculated explicitly but are expressed via a finite number of standard one-dimensional integrals (see [7]).

For regular grids of approximating nodes, the matrix of the discretized problem has the Toeplitz structure, and the FFT algorithms may be used for calculation of matrix-vector products by the iterative solution of the discretized problem. Note that the Toeplitz structure holds for any type of identical approximating functions and regular grids of approximating nodes.

There exist various ways of improvement of the numerical solution. As shown in [7], the Gaussian functions multiplied by special polynomials increase the accuracy of the approximation. If such functions are used in the framework of the method, the algorithm remains the same but the functions $\gamma_1,\ \gamma_2$ in Eqs. (25) and (26) will change. Note that there is a possibility to consider node grids with different steps $h_1,\ h_2,\ h_3$ in the directions $x_1,\ x_2,\ x_3$, and approximate the solution by "anisotropic" Gaussian functions. The action of the integral operator of the scattering problem on such functions (the analogy of the integral $\Gamma_{ij}(x)$ in Eq. (24)) is not calculated explicitly but is reduced to a finite number of standard one-dimensional integrals that can be tabulated.

Yet another advantage of the method is that it is well suited for parallel computations. For instance, the elements of the block-matrices in Eq. (34) and products of these matrices with vectors may be calculated independently and at the same time. This is another advantage of the method and a source of accelerating the computational process.

REFERENCES

1. Bohren, C. F. and D. R. Huffman, *Absorption and Scattering of Light by Small Particles*, John Wiley & Sons, NY, Toronto, Singapore, 1983.
2. Chew, W. C., J.-M. Jin, C.-C. Lu, E. Michielssen, and J. M. Song,

"Fast solution methods in electromagnetics," *IEE Transactions on Antennas and Propagation*, Vol. 45, No. 3, 533–543, 1997.

3. Tsang, L., J. A. Kong, K.-H. Ding, and C. O. Ao, *Scattering of Electromagnetic Waves: Numerical Solutions*, John Wiley & Sons, 2001.
4. Samokhin, A. B., *Integral Equations and Iterative Methods in Electromagnetic Scattering*, VSP, Utrecht, Boston, Koln, Tokyo, 2001.
5. Ewe, W.-B., L.-W. Li, and M.-S. Leong, "Solving mixed dielectric/conducting scattering problems using adaptive integral method," *Progress In Electromagnetics Research*, PIER 46, 143–163, 2004.
6. Fan, Z. H., R. S. Chen, H. Chen, and D. Z. Ding, "Weak form nonuniform fast Fourier transform method for solving volume integral equations," *Progress In Electromagnetics Research*, PIER 89, 275–289, 2009.
7. Maz'ya, V. anc G. Schmidt, *Approximate Approximation, Mathematical Surveys and Monographs*, Vol. 41, American Mathematical Society, Providence, 2007.
8. Kanaun, S. and S. B. Kochekseraii, "A numerical method for the solution of 3D-integral equations of electro-static theory based on Gaussian approximation functions," *Applied Mathematics and Computation*, Vol. 184, 754–768, 2007.
9. Peterson, A., S. Ray, and R. Mittra, *Computational Methods for Electromagnetics*, IEEE Press, NY, 1998.
10. Golub, G. and C. Van Loan, *Matrix Computations*, 3rd edition, The Johns Hopkins University Press, 1996.
11. Kanaun, S., "On the effective elastic properties of matrix composites: Combining the effective field method and numerical solutions for cell elements with multiple inhomogeneities," *International Journal of Engineering Sciences*, Vol. 48, No. 2, 160–173, 2009.